

Article

Vehicle Axle Load Identification Using Extracted Bridge Influence Line via Updated Static Component Technique

Pattarapong Asnachinda^{1,a,*} and Tospol Pinkaew^{2,b}

¹ Sustainable Civil Engineering and Infrastructure Research Unit, Department of Civil Engineering, Faculty of Engineering, Burapha University, Chonburi 20131, Thailand

² Department of Civil Engineering, Faculty of Engineering, Chulalongkorn University, Bangkok 10330, Thailand

E-mail: ^{a,*}pattarapong@eng.buu.ac.th (Corresponding author), ^btospol.p@chula.ac.th

Abstract. Bridge weigh-in-motion or moving force identification systems have been developed to screen the heavy truck or monitor its gross weight and axle loads. Bridge surface roughness has been considered a very sensitive parameter to the identification error. This paper presents the algorithm to accurately identify static axle weights by modifying the identification process to include the measured bridge influence line containing the actual road profile. The existing iterative calculation called the updated static component (USC) technique is also utilized to improve the dynamic axle load accuracy. The extracted influence line is obtained from a low-speed test using a known axle weight truck. Therefore, the characteristics of the road roughness and the measurement noise are included in the bridge responses. The effectiveness of the proposed technique is investigated through the numerical simulation and the experiment using scaled models. The results reveal that the identified axle loads become more accurate than those identified using the USC and the conventional regularized least squares methods. The proposed technique effectively decreases the identification errors of moving axle loads on the rough surface with a high measurement noise level. Moreover, the regularization parameter can be easily assigned with a broader range to achieve accurate identification results.

Keywords: Moving force identification, bridge weigh-in-motion, axle load, influence line.

ENGINEERING JOURNAL Volume 25 Issue 5

Received 27 September 2020

Accepted 12 April 2021

Published 31 May 2021

Online at <https://engj.org/>

DOI:10.4186/ej.2021.25.5.45

1. Introduction

The dynamic axle load and gross weight of vehicles are essential factors for designing new bridges and pavements, assessing the rating and fatigue life of existing roads and bridges, calibrating design codes and specifications, and controlling the heavy vehicles on highways. Monitoring the overweight trucks using weigh stations can only measure the static axle weight and the gross vehicle weight, and the truck is required to stop on the weighing scale. Hence, to directly measure the vehicle axle load's time-history without traffic disturbance, the weigh-in-motion (WIM) system was adopted. There are various types of WIM scales with different levels of accuracy. The existing technologies for WIM scales use measurement sensors such as bending plates, piezoelectric stripes, or load cells. However, these sensors are embedded in the pavement and disturb the traffic during installation and maintenance. Moses [1] presented an alternative system using an instrumented bridge as the scale to weigh the truck in motion called the bridge weigh-in-motion (B-WIM) system.

The original B-WIM employed the static influence line concept to calculate the predicted static axle weight and gross vehicle weight. However, traditional B-WIM can only estimate the static loads. Law et al. presented the moving force identification system (MFIS) based on the inverse problem of the relationship between moving force and bridge responses in a time-domain method [2], and a frequency and time domains analysis [3]. The MFIS applied the vehicle-bridge system's differential equation of motion to identify the time-varying axle loads simplified as a group of concentrated loads moving with a constant speed. The MFIS commonly uses acceleration, strain, and bending moment as the measurement responses. The major problem of the identification is that the system is an ill-posed problem. The identification result is very sensitive to measurement noise, in which the predicted load from a simple least squares becomes unrealistic due to large fluctuation at the location near the bridge's supports, especially to the solution from experimental studies [4, 5, 6]. A method of least squares with Tikhonov regularization was adopted to decrease the massive variation of identified moving force [7, 8]. The regularized least squares method requires the optimal regularization parameter determined from L-curve [9] to obtain an appropriate solution. However, constructing the L-curve requires numerous rounds of repetitive identification with the trial regularization parameters. Although the optimal regularization is applied, the predicted load time histories found from the experimental investigation are accurate only when all axles are close to midspan [7, 8, 10, 11]. With the singular value decomposition (SVD) technique, the regularized least squares method performs a robust solution at any regularization parameter [8, 12].

The updated static component (USC) technique [13] was proposed to overcome the difficulty of determining the optimal regularization parameter. The USC technique performs the iterative calculation to update the static load

component from the measured response, and the appropriate regularization parameter can be assigned at a broader range. Identification accuracy from experimental results was significantly improved through the time-histories of the identified forces [14, 15]. The estimation errors of static axle weight and gross vehicle weight obtained from the USC were smaller than the optimization using the theoretical response constructed from the concept of static influence line [16, 17].

O'Brien et al. [18] presented the determination of the actual influence line of bridge girders from the direct measurement using a calibrated vehicle. The B-WIM systems applying the extracted bridge influence line to Moses' algorithm [19, 20, 21] successfully enhance weight estimation accuracy. The directly measured influence line exhibits the bridge girder's actual characteristics subjected to the moving axle load.

Deng and Cai [22, 23] proposed axle load identification using the influence surface of deflection and strain responses for the deck slab and girder bridges. Road surface roughness and vehicle speed are the crucial parameters that influence the solution accuracy. Besides, accurate estimation of bridge influence line has been studied to increase the effectiveness of B-WIM [24, 25] and structural health monitoring of bridges [26].

Various studies on developed optimization processes such as the preconditioned conjugate gradient method [27], the redundant concatenated dictionary and weighted l1-norm regularization method [28], a comparison on the truncated generalized singular value decomposition (TGSVD), the piecewise polynomial truncated singular value decomposition (PP-TSVD), the modified preconditioned conjugate gradient (M-PCG), and the preconditioned least squares QR-factorization (PLSQR) methods [29] were presented to deal with the ill-condition of the MFIS. The results revealed the ability to decrease the identification error compared to the conventional regularized least squares method. However, the numerical simulation and experimental results were insufficient for verifying the identified dynamic load since the test provided only actual static force.

The straightforward optimization schemes have been adopted to identify the parameters of the moving vehicle, such as the genetic algorithm (GA) [30, 31], the artificial neural network (ANN) [32], and the virtual distortion method (VDM) [33]. They found that the vehicle mass can be identified with good accuracy with the presence of measurement noise and irregularity of road surface roughness. However, the optimization approaches based on the searching scheme require lots of training data and the upper and lower bounds or the initial trial values of all unknown parameters in the identification.

Recent research focused on developing the B-WIM and MFIS using modern instrumented sensors [34, 35] and the presence of multiple vehicles [35, 36]. Additionally, most recent studies concern the system implementation to the girder bridges, which are preferable for axle load identification with the free of axle detector (FAD) or the nothing-on-road (NOR) systems.

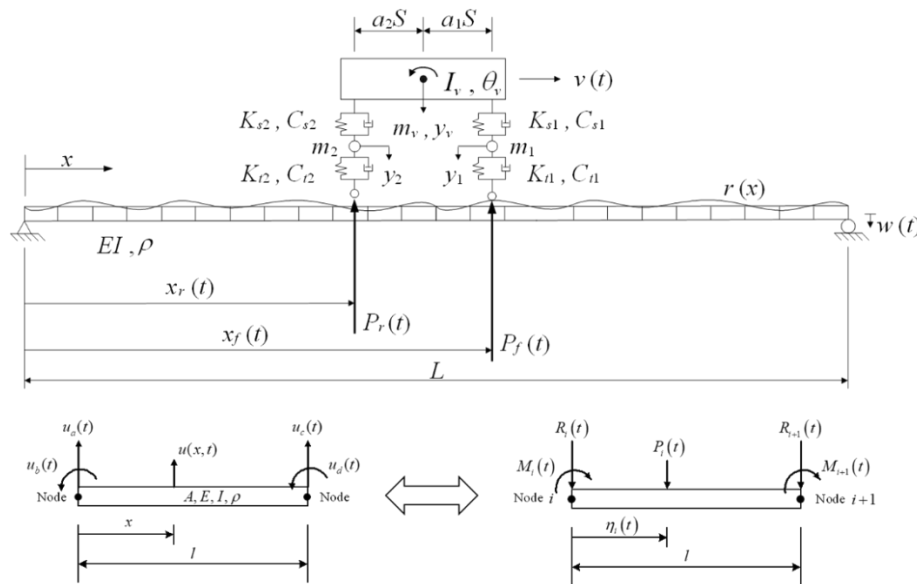


Fig. 1. Vehicle-bridge interaction system using a finite beam element model.

Regarding the review of previous studies, with the advantage of the USC technique and the use of extracted bridge influence line, the present study applied the benefit of the extracted bridge influence line to the USC technique to include the effects of bridge surface roughness and measurement noise. The regularized least squares optimization with the SVD method and the accuracy improvement scheme utilizing the extract bridge influence line via the iterative calculation based on the USC technique is proposed. Numerical examples through the computer simulation and experiment in the laboratory using the scaled vehicle-bridge model installed the actual wheel load detectors are investigated and discussed to evaluate the effectiveness of the proposed technique.

2. Theory of Vehicle-Bridge Interaction

2.1. Equation of Motion of Vehicle-Bridge System

Figure 1 shows a vehicle-bridge interaction system employing the finite element method. The vehicle is a four degree-of-freedom half-car considering the mass, damping, and stiffness of the suspensions and tires. Moving speed of the vehicle is denoted by $v(t)$. The bridge is discretized by Euler-Bernoulli beam elements. The equation of motion of the vehicle is represented as:

$$\begin{bmatrix} \mathbf{M}_{v1} & \mathbf{0} \\ \mathbf{0} & \mathbf{M}_{v2} \end{bmatrix} \ddot{\mathbf{Y}} + \begin{bmatrix} \mathbf{C}_{v11} & \mathbf{C}_{v12} \\ \mathbf{C}_{v21} & \mathbf{C}_{v22} \end{bmatrix} \dot{\mathbf{Y}} + \begin{bmatrix} \mathbf{K}_{v11} & \mathbf{K}_{v12} \\ \mathbf{K}_{v21} & \mathbf{K}_{v22} \end{bmatrix} \mathbf{Y} = - \begin{Bmatrix} \mathbf{0} \\ \mathbf{P}_{int} \end{Bmatrix} + \begin{Bmatrix} \mathbf{0} \\ \mathbf{M}_s \end{Bmatrix} \quad (1)$$

where \mathbf{M}_s is the static load vector of the vehicle; \mathbf{M}_{v1} , \mathbf{M}_{v2} , \mathbf{C}_{v11} , \mathbf{C}_{v12} , \mathbf{C}_{v21} , \mathbf{C}_{v22} , \mathbf{K}_{v11} , \mathbf{K}_{v12} , \mathbf{K}_{v21} , and \mathbf{K}_{v22} are respectively the mass, damping, and stiffness submatrices of the vehicle, and they are given in the Appendix.

$\mathbf{Y} = \{y_v, \theta_v, y_1, y_2\}^T$ is the response vector of the vehicle. $\mathbf{P}_{int} = \{P_f(t), P_r(t)\}^T$ is the interaction force vector represented in Eq. (2).

$$\begin{aligned} P_f(t) &= K_{t1}(y_1(t) - w(x_f(t), t) - r(x_f)) \\ &\quad + C_{t1}(\dot{y}_1(t) - w(x_f(t), t) + (m_1 + a_2 m_v)g) \\ P_r(t) &= K_{t2}(y_2(t) - w(x_r(t), t) - r(x_r)) \\ &\quad + C_{t2}(\dot{y}_2(t) - w(x_r(t), t) + (m_2 + a_1 m_v)g) \end{aligned} \quad (2)$$

where $r(x)$ is the road surface roughness at the location of tires. $x_f(t)$ and $x_r(t)$ are the positions of the front and rear axles respectively at time t . $w(x, t)$ is the vertical deflection of the bridge at the axle position x and time t , and g is the gravity acceleration. $y(t)$ and $\dot{y}(t)$ are the displacement and the velocity of the suspension mass, respectively. The equation of motion of the bridge is given as:

$$\mathbf{M}_b \ddot{\mathbf{R}} + \mathbf{C}_b \dot{\mathbf{R}} + \mathbf{K}_b \mathbf{R} = \mathbf{H} \cdot \mathbf{P}_{int} \quad (3)$$

where \mathbf{R} is the bridge nodal response vector. \mathbf{M}_b , \mathbf{C}_b and \mathbf{K}_b are the assembled mass, damping, and stiffness matrices of the bridge, respectively. The mass and stiffness matrices are formulated using the Hermitian cubic interpolation shape functions. The damping matrix is the modal damping in which the damping ratio is assumed to be equivalent for every vibration modes. \mathbf{H} is the load transformation matrix used to transform the axle load into the nodal force vector. The matrix \mathbf{H} contains the component shape function vectors of each interactive force. The shape function for the i^{th} interactive force on the j^{th} beam element is written as:

$$\mathbf{H}_{i,j}(x_i(t)) = \begin{Bmatrix} 1 - 3\left(\frac{\eta_i(t)}{l}\right)^2 + 2\left(\frac{\eta_i(t)}{l}\right)^3 \\ \eta_i(t)\left(\frac{\eta_i(t)}{l} - 1\right)^2 \\ 3\left(\frac{\eta_i(t)}{l}\right)^2 - 2\left(\frac{\eta_i(t)}{l}\right)^3 \\ \eta_i(t)\left(\left(\frac{\eta_i(t)}{l}\right)^2 - \frac{\eta_i(t)}{l}\right) \end{Bmatrix} \quad (4)$$

where l is the length of the beam element, $\eta_i(t)$ is the location of the i^{th} axle load referred from the left end of the j^{th} beam element expressed as $\eta_i(t) = x(t) - (j-1)l$. Bridge deflection at the position x at the time t can be calculated from:

$$w(x,t) = \mathbf{H}^T(x(t)) \cdot \mathbf{R}(t) \quad (5)$$

With the combination of Eq. (1) and Eq. (3), the equation of motion of the vehicle-bridge system can be formulated as follows:

$$\begin{bmatrix} \mathbf{M}_b & \mathbf{0} \\ \mathbf{0} & \mathbf{M}_v \end{bmatrix} \begin{Bmatrix} \ddot{\mathbf{R}} \\ \ddot{\mathbf{Y}} \end{Bmatrix} + \begin{bmatrix} \mathbf{C}_b + \mathbf{H} \cdot \mathbf{C}_n \cdot \mathbf{H}^T & -\mathbf{H} \cdot \mathbf{C}_t \\ -\mathbf{C}_t \cdot \mathbf{H}^T & \mathbf{C}_v + \mathbf{C}_t \end{bmatrix} \begin{Bmatrix} \dot{\mathbf{R}} \\ \dot{\mathbf{Y}} \end{Bmatrix} + \begin{bmatrix} \mathbf{K}_b + \mathbf{H} \cdot \mathbf{K}_n \cdot \mathbf{H}^T & -\mathbf{H} \cdot \mathbf{K}_t - v(t) \cdot \frac{\partial \mathbf{H}}{\partial x} \cdot \mathbf{C}_t \\ -\mathbf{K}_t \cdot \mathbf{H}^T - \mathbf{C}_t \cdot v(t) \cdot \frac{\partial \mathbf{H}^T}{\partial x} & \mathbf{K}_v + \mathbf{K}_t \end{bmatrix} \begin{Bmatrix} \mathbf{R} \\ \mathbf{Y} \end{Bmatrix} = \begin{Bmatrix} -\mathbf{H} \cdot \mathbf{K}_t \cdot \mathbf{r} + \mathbf{H} \cdot \mathbf{M}_s \\ -\mathbf{K}_t \cdot \mathbf{r} \end{Bmatrix} \quad (6)$$

where details of the sub-matrices in Eq. (6) are given in the Appendix. The step-by-step calculation using a discretizing method by state-space formulation [10] is used to determine the bridge and vehicle responses. In this study, the bridge surface roughness specified in ISO-8606 is adopted to simulate the magnitude of the road profile.

2.2. Bridge Strain Response

According to the derived nodal response of the bridge from Eq. (6), the bridge strain at the position on the beam x at the time t can be determined from Eq. (7).

$$\varepsilon(x,t) = -\gamma \frac{\partial^2 w(x,t)}{\partial x^2} \quad (7)$$

γ is the distance from the bottom surface of the bridge section to the neutral axis. Eq. (8) represents the strain response $z_j(t)$ at the j^{th} measuring point on the bridge calculated from the nodal displacements of the

corresponding beam element $u_a(t)$, $u_b(t)$, $u_c(t)$ and $u_d(t)$ as shown in Fig. 2.

$$z_j(\beta_j,t) = -\frac{\gamma}{l^3} \times \{12\beta_j - 6l \quad l(6\beta_j - 4l) \quad -12\beta_j + 6l \quad l(6\beta_j - 2l)\} \times \begin{Bmatrix} u_a(t) \\ u_b(t) \\ u_c(t) \\ u_d(t) \end{Bmatrix} \quad (8)$$

3. Vehicle Axle Load Identification

In the axle load identification system, since the axle loads of the vehicle are unknown; therefore the equation of motion of the vehicle-bridge interaction is replaced by the concept of a group of time-varying concentrated loads moving on a beam. Figure 3 represents the system of two-axle loads moving on a simply-supported bridge. The measured strain response \mathbf{Z} is defined as:

$$\mathbf{Z} = \{z_1(t) \quad z_2(t) \quad \dots \quad z_m(t)\}^T \quad (9)$$

where m is the number of measuring points, and $z_m(t)$ is the bridge strain response vector of the m^{th} measuring section. Similarly, the predicted strain response $\hat{\mathbf{Z}}$ containing m vectors of the theoretical bridge strain can be expressed as:

$$\hat{\mathbf{Z}} = \{\hat{z}_1(t) \quad \hat{z}_2(t) \quad \dots \quad \hat{z}_m(t)\}^T \quad (10)$$

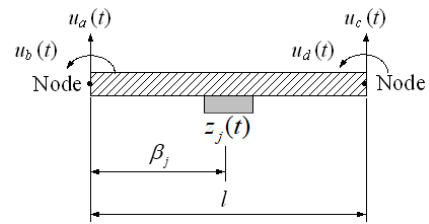


Fig. 2. Measuring point in a beam element.

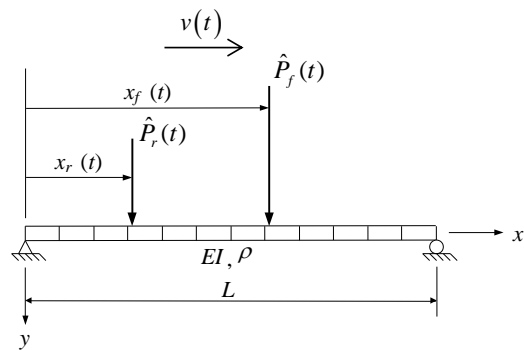


Fig. 3. Moving load-bridge system used in axle load identification.

3.1. Identification using Regularized Least Squares

The moving loads can be identified by the simple least squares method from the minimization of the residue between the measured and predicted bridge strain responses. However, using the simple least squares leads to the ill-conditioned solution, in which the obtained axle loads become unrealistic. The least squares function with Tikhonov regularization is therefore adopted to solve this ill-posed problem. Equation (11) represents the objective function of the identification system.

$$J(\hat{\mathbf{P}}, \lambda) = \|\mathbf{Z} - \hat{\mathbf{Z}}\|^2 + \lambda \|\hat{\mathbf{P}}\|^2 \quad (11)$$

where λ is the regularization parameter, and $\hat{\mathbf{P}}$ is the predicted interactive axle load. In this study, the theoretical bridge strain is formulated as the state variable vectors using state-space formulation as:

$$\hat{\mathbf{Z}} = \mathbf{Q}\hat{\mathbf{X}} \quad (12)$$

where \mathbf{Q} is the transformation matrix linking the relationship between the theoretical bridge strain and the state-variable vector of the bridge nodal response $\hat{\mathbf{X}} = [\mathbf{R} \ \dot{\mathbf{R}}]^T$. The identification using singular value decomposition (SVD) is also adopted to obtain a robust solution for any regularization parameter. The transformation matrix \mathbf{Q} is then decomposed to $\mathbf{Q} = \mathbf{U}\mathbf{\Sigma}\mathbf{V}^T$, in which \mathbf{U} and \mathbf{V} are orthogonal matrices of the decomposition, and $\mathbf{\Sigma}$ is the diagonal matrix containing singular values σ . The objective function becomes:

$$J(\hat{\mathbf{P}}, \lambda) = \sum_{i=1}^N \left[(\mathbf{z}_i - \mathbf{Q}\hat{\mathbf{X}}_i)^T (\mathbf{z}_i - \mathbf{Q}\hat{\mathbf{X}}_i) + \lambda \cdot \hat{\mathbf{P}}_i^T \hat{\mathbf{P}}_i \right] \quad (13)$$

where N is the number of time steps of the measured data, and $\hat{\mathbf{P}}_i = \{P_f \ P_r\}_i^T$ is the identified time-varying axle load vector containing the interaction force of the front and rear axles at the i^{th} time step. Hence, the solution of the predicted axle load vector $\hat{\mathbf{P}}$ is expressed as:

$$\hat{\mathbf{P}} = \sum_{k=1}^{NR} \left(\frac{\sigma_k}{\sigma_k^2 + \lambda} \right) \cdot (\mathbf{u}_k^T \mathbf{Z}) \mathbf{v}_k \quad (14)$$

where NR is the rank of the transformation matrix \mathbf{Q} . \mathbf{u}_k and \mathbf{v}_k are the sub-orthogonal vector of the matrices \mathbf{U} and \mathbf{V} , respectively.

3.2. Bridge Influence Line Extraction

The equivalent static axle weights of the vehicle can be estimated using the concept of the bridge influence line.

For an n -axle vehicle, Eq. (15) expresses the relationship between the theoretical bridge strain at the j^{th} measuring point and the n static axle weights.

$$\hat{\mathbf{Z}}_j = \sum_{i=1}^n \mathbf{I}\mathbf{L}_j^i \cdot \hat{P}_i^{\text{static}} \quad (15)$$

where predicted $\hat{P}_i^{\text{static}}$ is the static weight of the i^{th} axle. $\mathbf{I}\mathbf{L}_j^i$ is the vector of the bridge strain for the j^{th} measuring point containing the influence line ordinates with respect to the location of the i^{th} axle. The strain influence line vector of the bridge $\mathbf{I}\mathbf{L}_j$ can be determined using a calibrated truck with known axle weights. For a two-axle truck, the representation of Eq. (15) is given as:

$$\hat{\mathbf{Z}}_j = \left[\mathbf{I}\mathbf{L}_j^f \quad \mathbf{I}\mathbf{L}_j^r \right] \begin{Bmatrix} \hat{P}_f^{\text{static}} \\ \hat{P}_r^{\text{static}} \end{Bmatrix} \quad (16)$$

where $\mathbf{I}\mathbf{L}_j^f = \{\mathbf{I}\mathbf{L}_j \ \mathbf{0}\}^T$ and $\mathbf{I}\mathbf{L}_j^r = \{\mathbf{0} \ \mathbf{I}\mathbf{L}_j\}^T$ are the vectors of influence ordinate of the front and rear axles, respectively. $\mathbf{I}\mathbf{L}_j$ consists of the strain influence line ordinates for the whole bridge length at the j^{th} measuring point. From the calibration, the information on the location of each axle on the bridge is collected. Hence, the relationship between the measured bridge strain \mathbf{Z}_j and the influence line vector $\mathbf{I}\mathbf{L}_j$ of the j^{th} measuring section can be formulated as:

$$\mathbf{Z}_j = \mathbf{W}_j \mathbf{I}\mathbf{L}_j \quad (17)$$

where \mathbf{W}_j is the transition matrix containing the multiplication of the pre-weighted axle load and the location of the corresponding axle on the bridge. The recorded strain response used in Eq. (17) considers only the time step that the vehicle axle is on the bridge span; otherwise, the transition matrix \mathbf{W}_j becomes singular. Based on the inverse problem of Eq. (17), the strain influence line extracted from the direct measurement using the calibrated truck knowing its static axle weights can be determined from Eq. (18).

$$\mathbf{I}\mathbf{L}_j = (\mathbf{W}_j^T \mathbf{W}_j)^{-1} \mathbf{W}_j^T \mathbf{Z}_j \quad (18)$$

It is noted that factors directly related to the behavior of bridge strain, including moving speed, sampling frequency, road surface roughness, and measurement noise level, are crucial to the magnitude of the strain influence ordinates obtained from the direct measurement. This study utilizes the benefit of the extracted influence line to include the characteristics of the road profile and the measurement noise in the identification system.

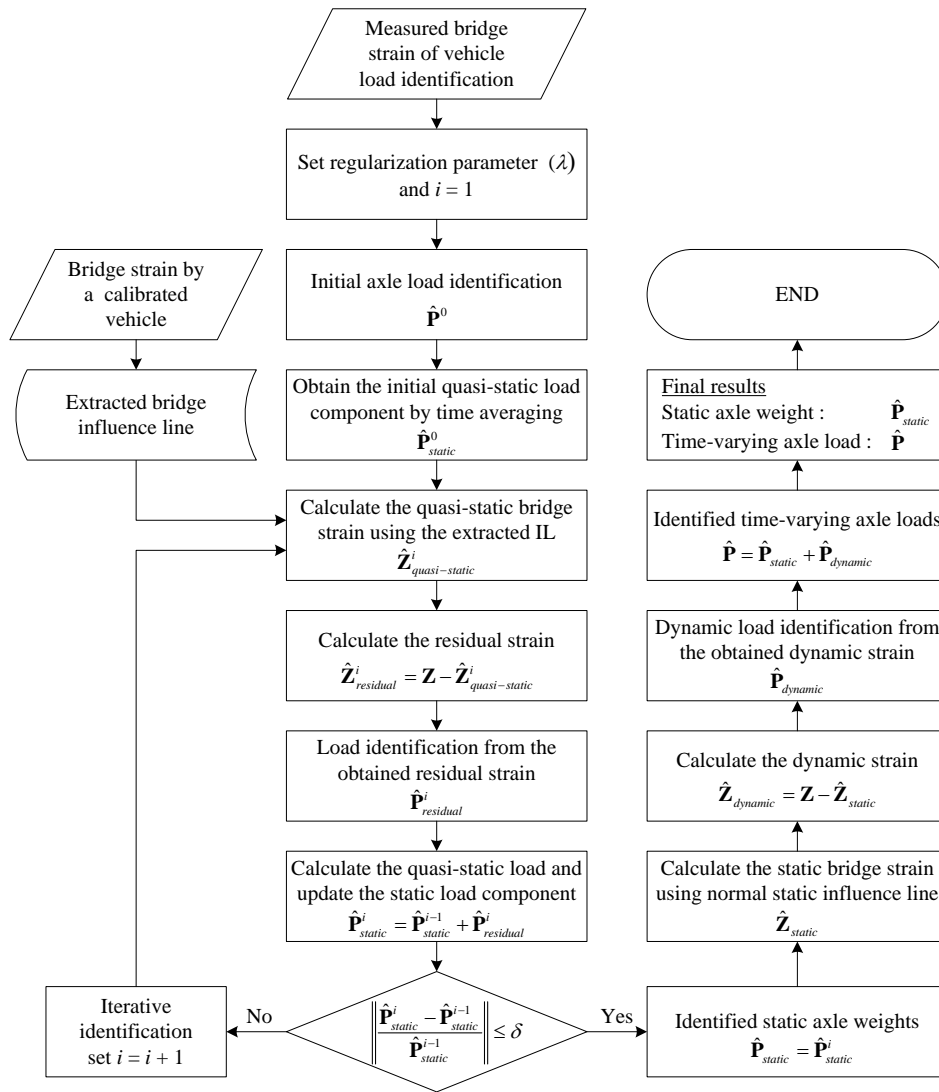


Fig. 4. Flow diagram of the identification algorithm.

However, the estimated static axle loads can vary by the moving speed. Traveling the calibrated truck at a crawling speed should be avoided because the effect of road roughness could vanish. The recommended vehicle speed in the calibration is between 3 - 10 m/s or nearly 10 - 35 km/hr approximately, which is convenient for the test. At this range, the measured strain response absorbs the vibration from the roughness profile, and the resolution of the influence line ordinates is higher than the high-speed test for the same sampling rate in data acquisition. The calibration using a heavy truck is preferable to increase the signal-to-noise ratio of the measured bridge response.

3.3. Modification of the Updated Static Component Technique

The updated static component technique (USC) [13] is the algorithm employing the iterative calculation of the static load component from time-averaging the identified axle loads in each round. The USC technique successfully improves the accuracy of the time-history of axle load, particularly when the vehicle axle is passing the bridge

supports. Besides, the iterative computation also eliminates the difficulty of the determination of an optimal regularization parameter. The regularization parameter can be selected in the broader range with a similar identification accuracy, and the identification error becomes smaller than the conventional regularized least squares solution.

This study presents the modification of the USC technique by replacing the system's static influence line with the extracted influence line. Additionally, based on the high accuracy of the static weight estimation using the influence line obtained from the direct measurement [18, 19, 20, 21], the modified USC approach identifies that static axle loads by using the residue between the measured and the quasi-static strain reconstructed from the extracted influence line as the input in each iteration. The iterative calculation of the static component updating finishes when the relative difference of the latest and the previously identified static loads is smaller than the tolerance δ . The tolerance is set as 1% according to the previous studies employing the USC technique [14, 15]. Once the updated static axle load converges to the final solution, the dynamic load component will be computed

in the last process from the dynamic strain, which is the residue from the subtraction of the measured bridge strain by the static bridge strain reconstructed from the typical static influence line concept. The extracted influence line is no longer used in the static strain reconstruction process because it contains the bridge's dynamic characteristics due to road roughness and moving speed. Finally, the time-varying axle load is accomplished by combining the identified static and dynamic axle loads. Figure 4 shows the flow diagram of the proposed identification algorithm. The identification accuracy is investigated through the static weight error of the static axle weight and the relative percentage error (RPE) of the time-varying axle load defined by Eq. (19) and Eq. (20), respectively.

$$\text{Static weight error} = \left(\frac{\hat{P}_{static}^i - P_{static}^i}{P_{static}^i} \right) \times 100\% \quad (19)$$

where \hat{P}_{static}^i and P_{static}^i are the identified and actual static weights of the i^{th} axle, respectively. The positive and negative signs of the static weight error denote the overestimated and underestimated values, respectively.

$$RPE = \frac{\|\hat{\mathbf{P}}_i - \mathbf{P}_i\|}{\|\mathbf{P}_i\|} \times 100\% \quad (20)$$

where $\hat{\mathbf{P}}_i$ and \mathbf{P}_i represent the vectors of the i^{th} identified and actual time-varying axle loads, respectively.

Table 1. Parameters of the simulated vehicle-bridge system.

Vehicle-bridge properties			
$L = 30$ m	$EI = 2.5 \times 10^{10}$ N·m ²	$\rho A = 5000$ kg/m	$\xi = 0.02$ for all modes
$I_v = 1.47 \times 10^5$ kg·m ²	$m_v = 17,735$ kg	$m_1 = 1,500$ kg	$m_2 = 1,000$ kg
$k_{s1} = 2.47 \times 10^6$ N/m	$k_{s2} = 4.23 \times 10^6$ N/m	$k_{r1} = 3.74 \times 10^6$ N/m	$k_{r2} = 4.60 \times 10^6$ N/m
$c_{s1} = 3.00 \times 10^4$ N/m	$c_{s2} = 4.00 \times 10^4$ N/m	$c_{r1} = 3.90 \times 10^3$ N/m	$c_{r2} = 4.30 \times 10^3$ N/m
$S = 4.27$ m	$a_1 = 0.519$	$a_2 = 0.481$	

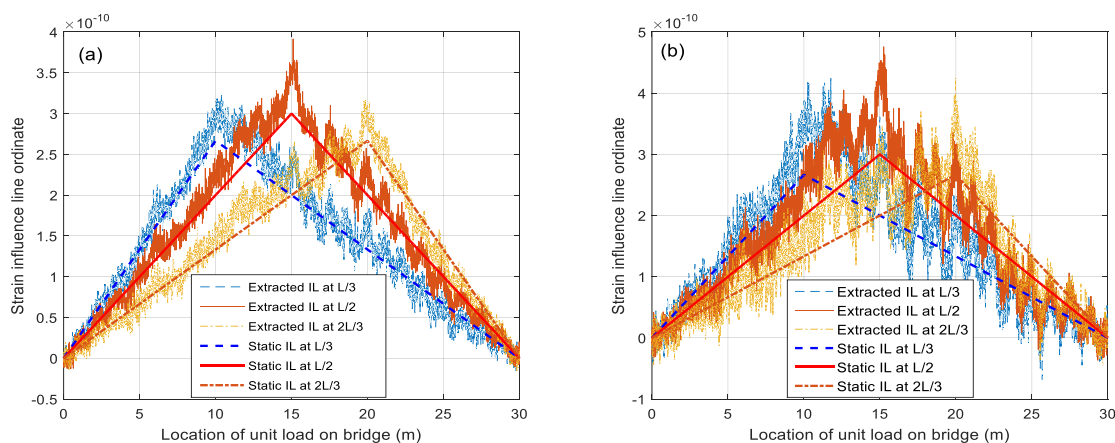


Fig. 5. Influence line extraction: (a) roughness level II and 5% noise level (b) roughness level III and 10% noise level.

4. Numerical Simulation

The vehicle-bridge interaction system employing the finite element method was conducted for numerical simulation. The bridge was modeled as a single-span simply supported beam with a span length of 30 m. The vehicle was a two-axle truck with an axle spacing of 4.27 m. The simulation employed the physical properties of the truck-bridge system. Table 1 lists the vehicle-bridge parameter, which was also used in previous studies [11, 15]. Bridge strain response was simulated from the bridge model discretized for 32 beam elements. According to the previous research works, the identification system assembled the bridge using eight beam elements [11, 17]. The sampling frequency was set at 200 Hz. The truck model traveled across the bridge with different surface roughness at a constant speed. The simulated road roughness profile using ISO-8606 in this study was classified into three levels inducing various dynamic amplification factors to the axle load. The road roughness levels I, II, and III generated the maximum impact factor to the axle load of 10%, 20%, and 40%, respectively. Besides, since the extracted bridge influence line must be unique for the instrumented bridge with the inclusion of the actual road profile, the surface roughness used in the response simulation and the influence line extraction is precisely the same profile for each scenario. Strain responses were collected from three measuring points located on the bridge sections at $L/3$, $L/2$, and $2L/3$.

The influence line used in the identification was extracted from the pre-weighted truck moving at a constant speed of 5 m/s. The calibrated truck has the same properties as the vehicle in Table 1 but the gross weight is heavier from the additional mass of 10,000 kg. Fig. 5 shows the comparison of the general static influence line and the extracted influence lines. It is indicated that the shape of the obtained influence lines is different from the static influence line due to the vehicle dynamics, road profile, and measurement noise. The variation between the extracted and the static influence ordinates becomes larger with the higher roughness and noise levels.

Fig. 6 compares the identification results using the conventional regularization, the regularization with the USC technique, and the proposed algorithm in case of a truck moves on the surface roughness level III at a 15

m/s with a noise level of 10%. It is indicated that the proposed method performs the most accurate results among the three approaches, particularly to the static weight determination. Moreover, the static weight estimation using a regularization parameter between 0.01 to 1000 performs the identification error below 10% for every axle.

The identification error for the time-varying axle load by the proposed method is slightly lower than those obtained from the USC technique. The optimal regularization parameter for dynamic load identification for the USC and the proposed schemes seem similar. However, the proposed method requires many loops of the iteration when a wrong regularization parameter is assigned. Consequently, the appropriate regularization parameter can be selected based on the number of computational rounds.

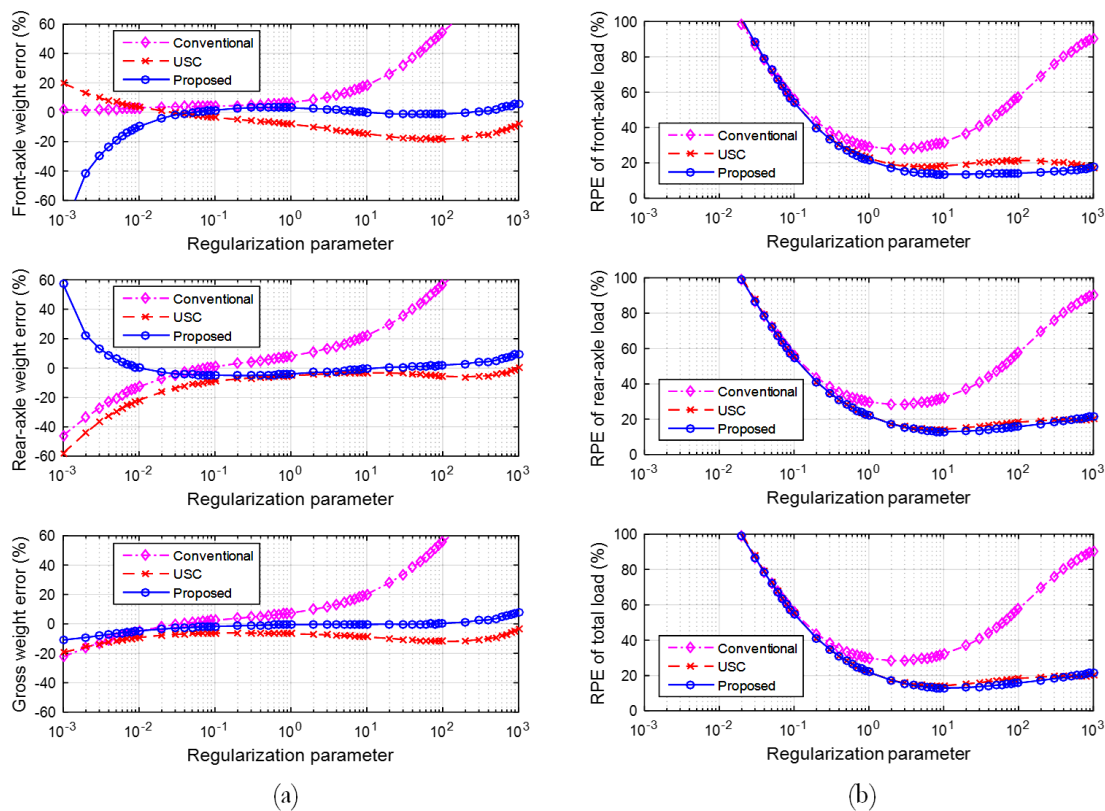


Fig. 6. Regularization parameter on the identification error for roughness level III and 10% noise level: (a) static weight and (b) time-varying load.

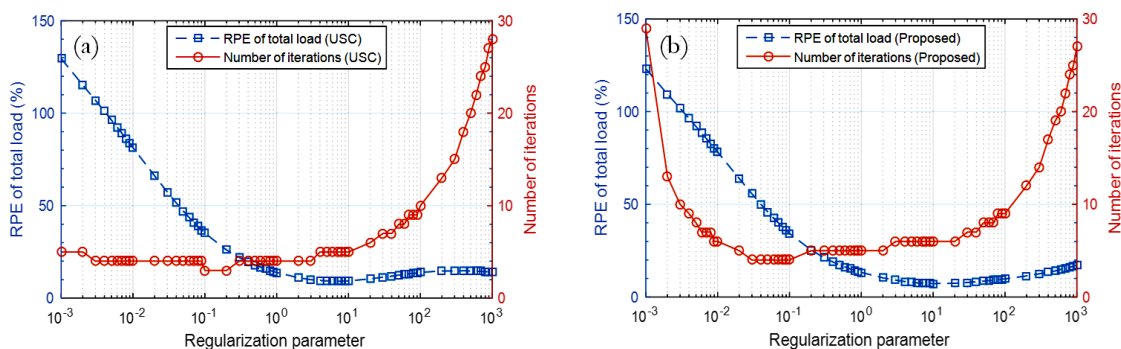


Fig. 7. RPE of total load and number of iterations for roughness level III and 10% noise level: (a) USC (b) proposed.

Table 2. Identification result of numerical examples.

Case	1	2	3	4	5	6	7
Total vehicle mass (kg)	25,235	25,235	25,235	20,235	20,235	30,235	30,235
FGR	0.40	0.40	0.40	0.50	0.50	0.30	0.30
Moving speed (m/s)	20	20	20	25	25	15	15
Roughness level	I	II	III	I	III	I	III
Measurement noise level (%)	1	5	10	1	5	1	10
USC technique ($\lambda = 10$)							
Static weight error of front-axle (%)	-10.15	-14.36	-22.18	-5.08	-16.16	-9.62	-27.25
Static weight error of rear-axle (%)	3.44	3.89	2.90	0.47	-1.48	1.99	3.28
Static gross weight error (%)	-2.00	-3.41	-7.13	-2.28	-8.76	-1.49	-5.88
RPE of front-axle load (%)	11.28	15.68	24.55	5.78	17.65	10.73	29.35
RPE of rear-axle load (%)	7.01	8.18	11.73	7.12	14.27	5.56	9.88
RPE of total load (%)	3.20	4.57	8.18	2.57	8.08	2.25	7.12
Number of iterations	8	7	6	5	6	14	12
Proposed technique ($\lambda = 10$)							
Static weight error of front-axle (%)	-7.86	-9.19	-7.22	-3.38	-6.63	-6.67	-9.64
Static weight error of rear-axle (%)	3.87	4.29	2.61	1.08	1.19	2.34	4.04
Static gross weight error (%)	-0.82	-1.11	-1.33	-1.13	-2.69	-0.36	-0.06
RPE of front-axle load (%)	11.31	13.73	17.43	8.55	15.59	10.16	20.91
RPE of rear-axle load (%)	6.59	7.33	10.17	7.03	13.00	5.33	8.44
RPE of total load (%)	4.00	4.50	6.73	3.88	6.94	3.77	5.94
Number of iterations	9	9	10	6	6	15	14

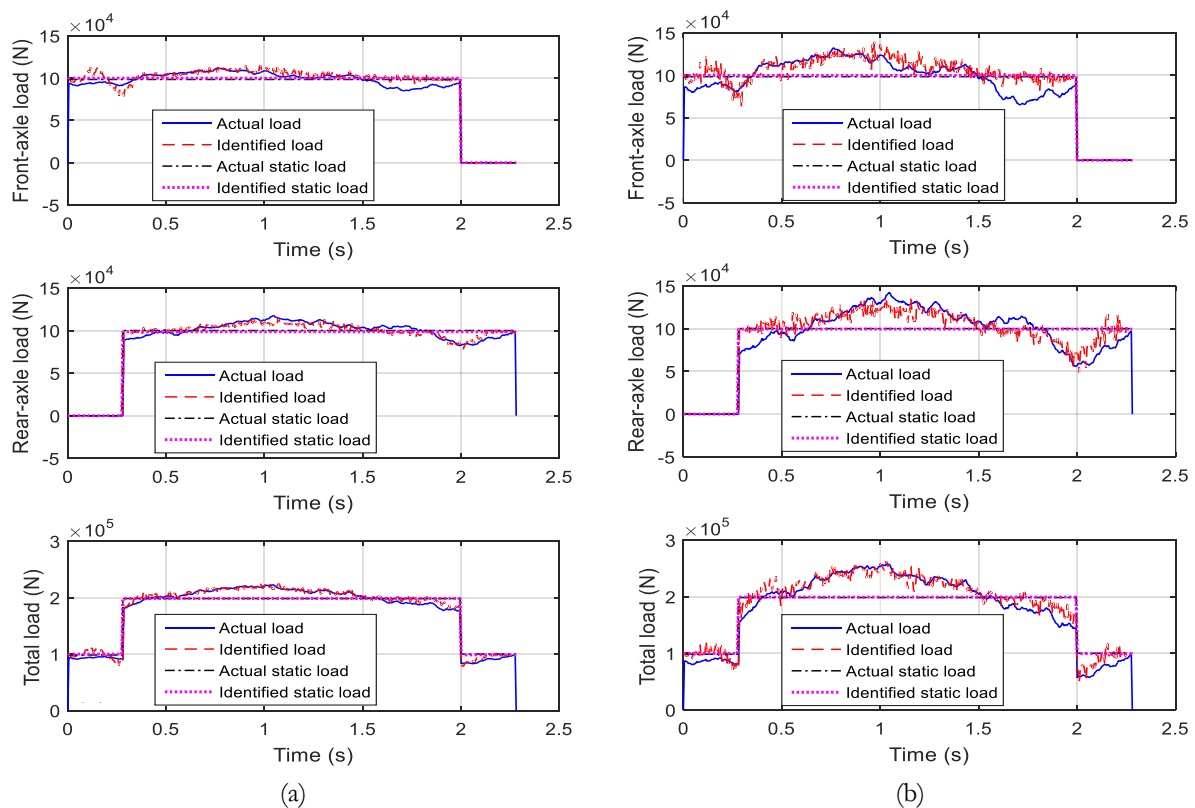


Fig. 8. Identified load: (a) roughness level II and 5% noise level and (b) roughness level III and 10% noise level.

Table 2 lists the identification results from numerical examples of various factors, in which the regularization parameter is simply set as 10 for every

scenario. It is found that the proposed technique decreases the identification error in both static and dynamic loads for all cases.

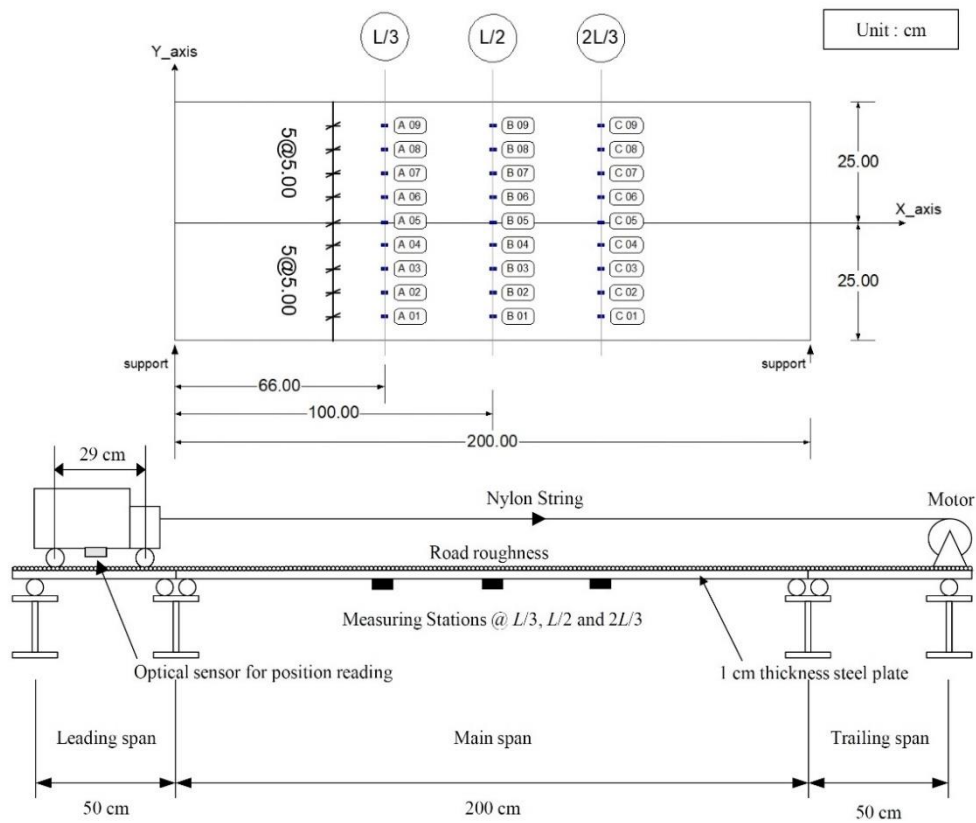


Fig. 9. Bridge model.

The numerical results reveal that applying the extracted influence line to the computation improves the accuracy of the estimated static weight effectively, particularly to the bridge having a high road roughness level. The errors of the static axle weight and the static gross weight are all below 10% and 3%, respectively. It is observed that the RPE of the dynamic load becomes smaller except for the cases having both road roughness and measurement noise of level I, which are slightly larger. Different moving speed and front axle weight to the gross weight ratio (FGR) of a truck are less sensitive to the solution accuracy compared to the road profile. Figure 8 demonstrates the time histories of the identified axle and total loads from case 2 and case 3, in which the computed forces perform in a good match to the actual forces for both cases.

5. Experimental Verification

5.1. Experimental Setup

The experimental study was conducted through the vehicle-bridge model, in which the bridge span length and the axle spacing of the two-axle car model were designed on a scale of 1:15. Figure 9 illustrates the experimental setup. The simply-support bridge with a span length of 2 m fabricated from steel plate was modeled from the full-scale bridge with a span length of 30 m. From the free vibration test, the natural frequency and the damping ratio of the bridge were 5.5 Hz and 0.005, respectively. The car

model was a two-axle truck with an axle spacing of 0.29 m, which was scaled from the H20 truck having an axle spacing of 4.27 m. Strain signals were measured from three sections at locations of $L/3$, $L/2$, and $2L/3$. Twenty-seven strain gauges were installed at the bottom bridge surface. The response used in the identification system for each measuring point was the average value of the nine sensors mounted with a gradually spacing.

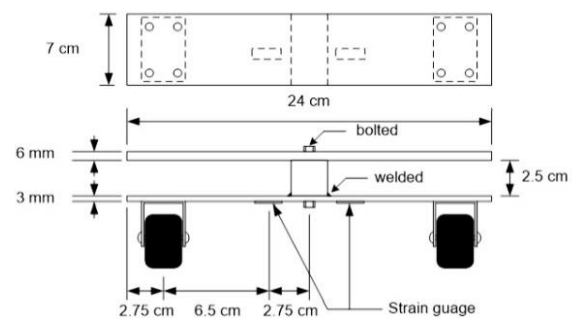


Fig. 10. Instrumented vehicle model.

The vehicle model installed an optical sensor to detect the axle position at every 0.5 cm from the reading of black-white stripes attach on the road. Figure 10 shows the car model, which the axle load detectors were equipped. The instruments were designed and calibrated from the strain reading at the suspension arms and wheel forces.

The data acquisition system recorded the signal from all sensors at a sampling rate of 256 Hz. Measurement noise filtering is recommended, although it is included in the influence line obtained from the direct measurement. The acquired signals were filtered the measurement noise using the simple moving average as a low-pass filter. In addition to the smooth bridge surface, the road with a rough profile was also considered in the test. The artificial road roughness was made by placing a group of wooden sticks having a circular section with a diameter of 0.5 cm along the moving path.

5.2. Influence Line Extraction

For the influence line extraction, the direct measurement using the calibrated vehicle was conducted. The calibrated model was a 30-kg mass of two-axle car moving at an average speed of 0.25 m/s equivalent to the full-scale as 3.75 m/s or 13.5 km/hr. The strain influence ordinate obtained from the calibration was interpolated for the position every 1 cm along the bridge span. It is observed that the extracted influence line of bridge strains exhibits the dynamics from the road roughness and low-speed movement of the calibrated truck. Figure 11 shows the extracted influence lines from the smooth and rough bridges.

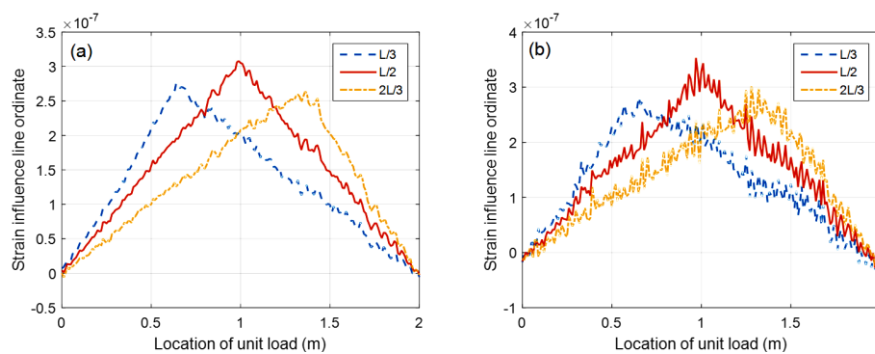


Fig. 11. Extracted influence line of the bridge model (a) smooth surface (b) rough surface.

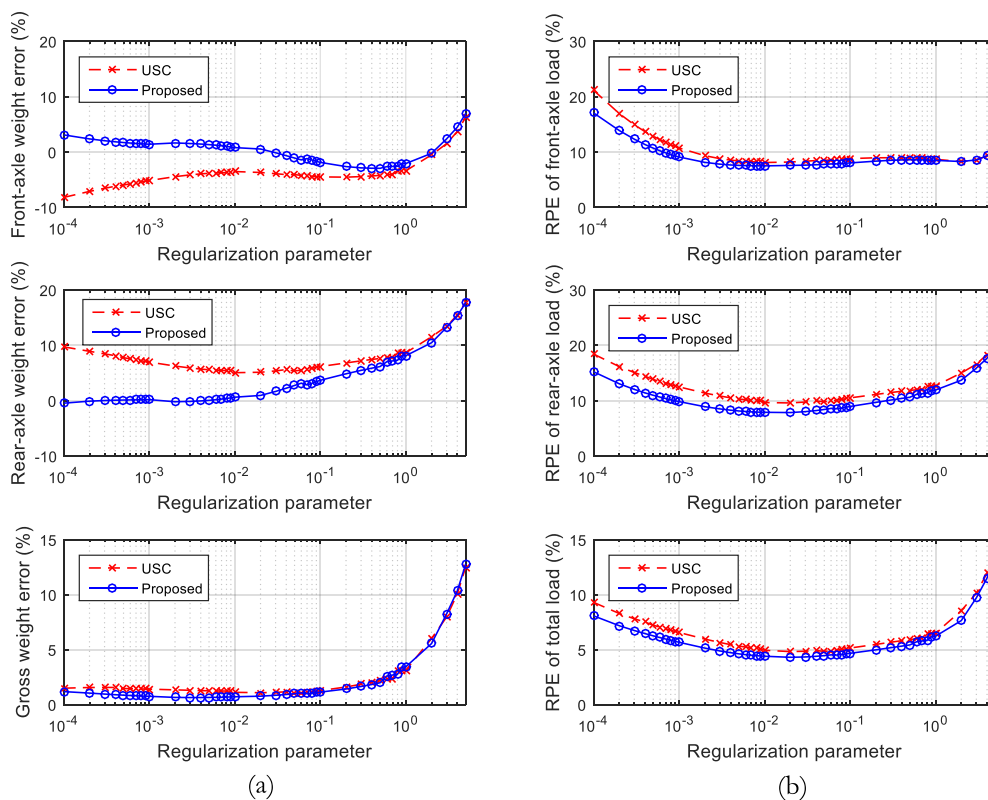


Fig. 12. Regularization parameter on the identification error of the 20-kg vehicle moving on a smooth bridge at an average speed of 0.92 m/s: (a) static weight error and (b) RPE of time-varying load.

5.3. Regularization Parameter

Figure 12 shows the example of the identification error of the 20-kg truck moving on a smooth surface bridge at an average speed of 0.92 m/s. The plots reveal the sensitivity of the regularization to the solution accuracy computed by the USC and proposed algorithms. It is indicated that the modified approach accurately identifies both the static and dynamic loads. The static weight errors significantly decrease for every axle and also vehicle gross weight. The dynamic load errors become smaller at every value of the regularization parameter, where the optimal parameter is observed at nearly 0.01.

For the conventional regularized least squares optimization, the optimal regularization parameter can be determined using L-curve [9]. However, L-curve requires a considerable number of repetitive identification than the USC and the proposed algorithm to create the plot and determine the optimal point located at the maximum curvature. Besides, the optimal regularization parameter is unique for each case from many relevant properties of the vehicle-bridge system. Hence, using a specific regularization parameter in the identification algorithm for every predicted vehicle is preferable in practice. The selected regularization parameter used in the experimental study was 0.01 for all cases. Table 3 lists the identification result from eight experimental scenarios varying various parameters including vehicle mass, front axle weight to gross weight ratio (FGR), moving speed, and bridge surface roughness. Identification errors obtained from the proposed algorithm and the USC technique were

compared to investigate the effectiveness of the improved method.

5.4. Experimental Results

Regarding the experimental results listed in Table 3, the obtained result reveals that the identification using the extracted influence line via the USC technique provides more accurate results than the ordinary USC technique for every case. For the cases with a smooth surface bridge, the maximum errors of static axle weight and static gross weight significantly decrease to below $\pm 4\%$ and $\pm 2\%$, respectively. The predicted dynamic loads perform slightly better than those obtained from USC. The identification errors of the time-varying axle load and total load from the experiment are less than 9% and 5%, respectively. This is because a vehicle moving with faster speed induces more dynamics to the axle force, which leads to higher identification errors.

For the effect of bridge surface roughness, the results from the last four cases in Table 3 indicate that the estimated static and dynamic loads perform larger identification errors than the smooth surface bridge. The proposed algorithm accurately updates the identified static axle weight. Moreover, the relative percentage errors of the predicted dynamic axle loads are also reduced. The vehicle speed seems to have more effect on the identification error than the vehicle mass. This is because the extracted influence line obtained from the direct measurement was conducted at a low speed.

Table 3. Identification result from the experiment.

Case	1	2	3	4	5	6	7	8
Total vehicle mass (kg)	20	30	20	30	20	30	20	30
FGR	0.46	0.44	0.46	0.45	0.43	0.45	0.43	0.44
Average speed (m/s)	0.48	0.47	0.92	0.96	0.87	0.99	1.28	1.19
Bridge surface	smooth	smooth	smooth	smooth	rough	rough	rough	rough
USC technique ($\lambda = 0.01$)								
Static weight error of front-axle (%)	-1.88	-8.65	-3.65	-7.84	-8.15	-7.99	-14.95	-12.05
Static weight error of rear-axle (%)	4.84	4.81	5.38	4.89	5.29	12.33	15.33	13.74
Static gross weight error (%)	1.75	-1.06	1.23	-0.81	-0.43	3.28	2.21	2.45
RPE of front-axle load (%)	5.62	9.67	8.22	10.72	18.18	16.39	25.88	18.66
RPE of rear-axle load (%)	6.23	6.15	9.88	9.48	16.76	18.06	26.78	21.51
RPE of total load (%)	2.93	2.04	5.03	4.26	9.27	9.23	12.94	10.62
Number of iterations	4	5	4	4	5	4	4	4
Proposed technique ($\lambda = 0.01$)								
Static weight error of front-axle (%)	2.80	-3.71	0.81	-3.41	-2.88	-4.44	-11.19	-8.93
Static weight error of rear-axle (%)	0.12	0.30	0.63	0.44	-3.35	4.52	7.53	5.81
Static gross weight error (%)	1.35	-1.45	0.71	-1.28	-3.15	0.53	-0.58	-0.64
RPE of front-axle load (%)	5.49	5.98	7.51	8.26	15.91	14.44	23.76	16.14
RPE of rear-axle load (%)	3.69	3.51	7.90	7.43	16.18	15.05	24.40	19.05
RPE of total load (%)	2.35	1.62	4.40	3.59	9.70	8.36	12.41	9.85
Number of iterations	6	6	6	6	7	6	6	6

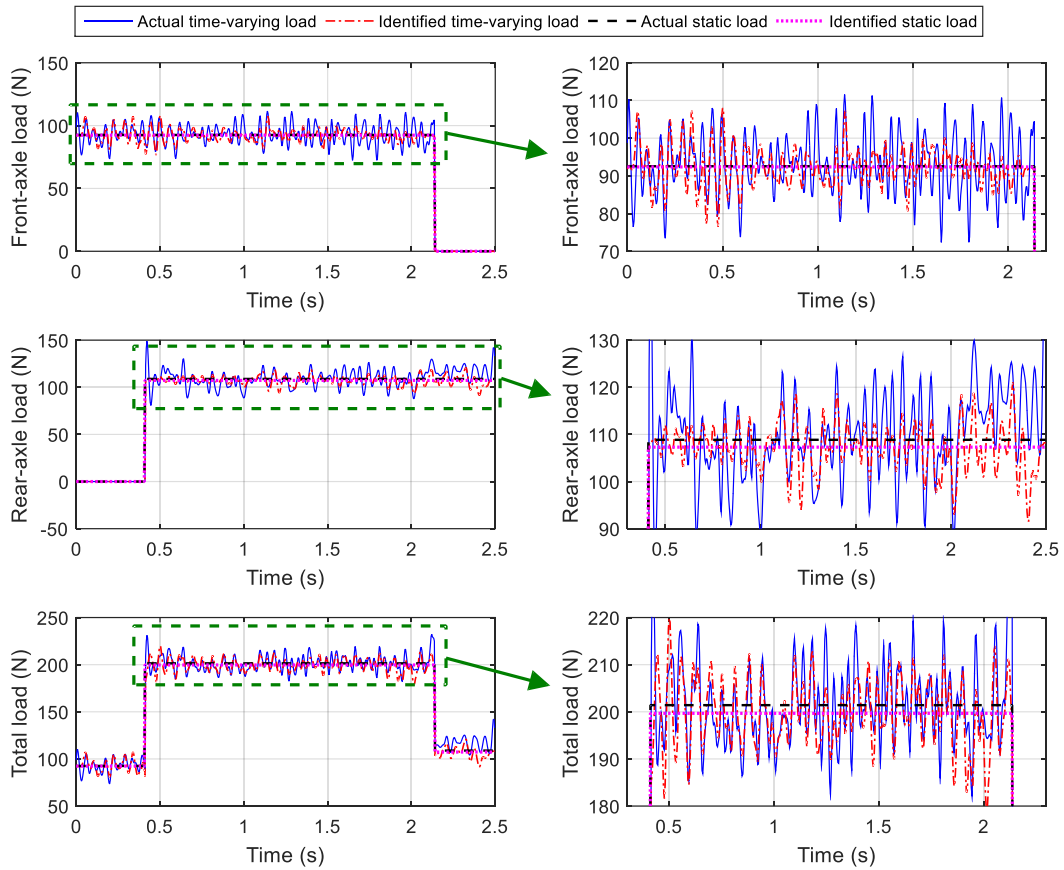


Fig. 13. Identified loads of the experiment on the smooth surface bridge (case 3).

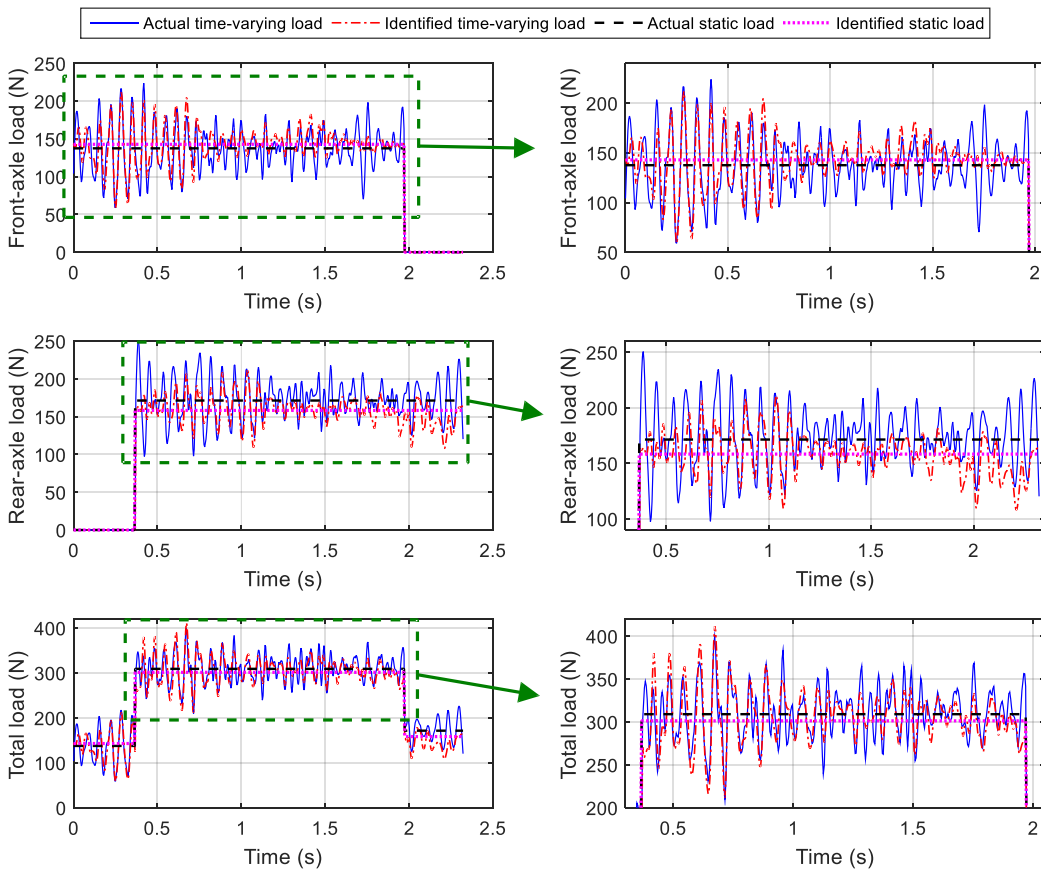


Fig. 14. Identified loads of the experiment on the rough surface bridge (case 6).

However, using a high-speed test of influence line extraction should be avoided. If the influence ordinate includes identical dynamics from the high moving speed of the calibrated vehicle, the system will accurately identify only a vehicle having similar physical properties to the calibrated car. The proposed method requires only a couple of additional iteration compared to the USC technique to accomplish an accurate solution. Figures 13 and Fig. 14 show the time histories of the actual and identified time-varying loads for case 3 and case 6, respectively. The predicted forces exhibit an excellent matching to the real forces, especially to the total load for both smooth and rough road profiles.

The results discussed above use the same regularization parameter of 0.01 obtained from Fig. 12. Although the static weight can be accurately estimated, the actual dynamic axle loads are unknowns in practice. Therefore, a specific regularization parameter assigned in the implemented identification system can be determined from L-Curves of the preliminary test using various mass of the pre-weight trucks. The identification error from a high-speed vehicle can be controlled in practice by speed limit enforcement or selecting the instrumented bridge locating in a low-speed area. Moreover, it is noted that the recalibration of the extracted bridge influence line is highly recommended when the pavement or structural component of the bridge is repaired or reconstructed.

6. Conclusions

The vehicle axle load identification from the bridge strain response is analytically and experimentally studied. This research presents the improved identification algorithm employing the strain influence line extracted from the direct measurement and the iterative calculation via the updated static component (USC) technique. The proposed method's accuracy and effectiveness are investigated and compared to the conventional regularized least squares and the USC methods. The analytical results obtained from the numerical simulation indicate that the proposed approach accurately identifies static axle weight and static gross weight with a broader range of the regularization parameter compared to the USC technique. The modified algorithm also provides the lower identification error of the dynamic axle loads, especially for a high measuring noise level and high magnitude of bridge surface roughness. This is because the extracted strain influence line includes the dynamics of the road profile and measurement noise. The regularization parameter can be selected concerning the appropriate number of computational loops of the system.

The experimental verification using scaled models also reveals that the proposed algorithm can provide better identification results than the USC for every scenario. The identified time-varying load exhibits an excellent matching to the measured actual axle force. The calculation requires only a couple of additional iteration compared to the USC. For a smooth surface bridge, the maximum errors of the static weight estimation are below

$\pm 4\%$ and $\pm 2\%$ for the axle weight and gross weight, respectively. The relative percentage errors of the dynamic loads are less than 9% and 5% for the axle load and total load, respectively. However, the axle loads of a vehicle moving on the rough road surface at high speed becomes difficult to be accurately identified.

For the system implementation, since the actual axle loads are unknown, the appropriate regularization parameter can be selected from the bridge test under the pre-weight trucks. The advantage of the proposed method is that the optimal regularization parameter, which is usually very sensitive to vehicle-bridge parameters, can be easily assigned. To decrease the identification error of high-speed trucks in practice, speed control enforcement or selecting the instrumented bridge locating in a low-speed area is recommended. Regarding the proposed method's effectiveness in both analytical and experimental studies, future research on the full-scale application is being investigated. It is expected that the proposed algorithm is an attractive alternative to existing methods for bridge weigh-in-motion systems.

Acknowledgements

The authors are very grateful for the financial support to this work under the research and development fund from the Faculty of Engineering, Burapha University (no. 78/2552).

Appendix

$$\begin{aligned} \mathbf{M}_{v1} &= \begin{bmatrix} m_v & 0 \\ 0 & I_v \end{bmatrix}; & \mathbf{M}_{v2} &= \begin{bmatrix} m_1 & 0 \\ 0 & m_2 \end{bmatrix}; \\ \mathbf{M}_s &= \begin{Bmatrix} (m_1 + a_2 m_v) g \\ (m_2 + a_1 m_v) g \end{Bmatrix}; & \mathbf{r} &= \begin{Bmatrix} r(x_f(t)) \\ r(x_r(t)) \end{Bmatrix}; \\ \mathbf{C}_{v11} &= \begin{bmatrix} C_{s1} + C_{s2} & (-C_{s1} a_1 + C_{s2} a_2) S \\ (-C_{s1} a_1 + C_{s2} a_2) S & (C_{s1} a_1^2 + C_{s2} a_2^2) S^2 \end{bmatrix}; \\ \mathbf{C}_{v12} &= \begin{bmatrix} -C_{s1} & -C_{s2} \\ C_{s1} a_1 S & -C_{s2} a_2 S \end{bmatrix}; \\ \mathbf{C}_{v21} &= \begin{bmatrix} -C_{s1} & C_{s1} a_1 S \\ -C_{s2} & -C_{s2} a_2 S \end{bmatrix}; & \mathbf{C}_{v22} &= \begin{bmatrix} C_{s1} & 0 \\ 0 & C_{s2} \end{bmatrix}; \\ \mathbf{K}_{v11} &= \begin{bmatrix} K_{s1} + K_{s2} & (-K_{s1} a_1 + K_{s2} a_2) S \\ (-K_{s1} a_1 + K_{s2} a_2) S & (K_{s1} a_1^2 + K_{s2} a_2^2) S^2 \end{bmatrix}; \\ \mathbf{K}_{v12} &= \begin{bmatrix} -K_{s1} & -K_{s2} \\ K_{s1} a_1 S & -K_{s2} a_2 S \end{bmatrix}; \\ \mathbf{K}_{v21} &= \begin{bmatrix} -K_{s1} & K_{s1} a_1 S \\ -K_{s2} & -K_{s2} a_2 S \end{bmatrix}; & \mathbf{K}_{v22} &= \begin{bmatrix} K_{s1} & 0 \\ 0 & K_{s2} \end{bmatrix}; \\ \mathbf{C}_t &= \begin{bmatrix} 0 & 0 & 0 & 0 \\ 0 & 0 & 0 & 0 \\ 0 & 0 & C_{t1} & 0 \\ 0 & 0 & 0 & C_{t2} \end{bmatrix}; & \mathbf{K}_t &= \begin{bmatrix} 0 & 0 & 0 & 0 \\ 0 & 0 & 0 & 0 \\ 0 & 0 & K_{t1} & 0 \\ 0 & 0 & 0 & K_{t2} \end{bmatrix}; \\ \mathbf{C}_u &= \begin{bmatrix} C_{t1} & 0 \\ 0 & C_{t2} \end{bmatrix}; & \mathbf{K}_u &= \begin{bmatrix} K_{t1} & 0 \\ 0 & K_{t2} \end{bmatrix} \end{aligned}$$

References

- [1] F. Moses, "Weigh-in-motion system using instrumented bridges," *Journal of Transportation Engineering*, vol. 105, no. 3, pp. 233-249, 1979.
- [2] S. S. Law, T. H. T. Chan, and Q. H. Zheng, "Moving force identification: A time domain method," *Journal of Sound and Vibration*, vol. 201, no. 1, pp. 1-22, 1997.
- [3] S. S. Law, T. H. T. Chan, and Q. H. Zheng, "Moving force identification: A frequency and time domain analysis," *Journal of Dynamic Systems, Measurement, and Control ASME*, vol. 121, no. 3, pp. 394-401, 1999.
- [4] T. H. T. Chan, S. S. Law, T. H. Yung, and X. R. Yuan, "An interpretive method for moving force identification," *Journal of Sound and Vibration*, vol. 219, no. 3, pp. 503-524, 1999.
- [5] X. Q. Zhu and S. S. Law, "Identification of vehicle axle loads from bridge dynamic response," *Journal of Sound and Vibration*, vol. 236, no. 4, pp. 705-724, 2000.
- [6] T. H. T. Chan, S. S. Law, and T. H. Yung, "Moving force identification using an existing prestressed concrete bridge," *Engineering Structures*, vol. 22, no. 10, pp. 1261-1270, 2000.
- [7] S. S. Law, T. H. T. Chan, Q. X. Zhu, and Q. H. Zeng, "Regularization in moving force identification," *Journal of Engineering Mechanics ASCE*, vol. 127, no. 2, pp. 136-148, 2001.
- [8] X. Q. Zhu and S. S. Law, "Moving loads identification through regularization," *Journal of Engineering Mechanics ASCE*, vol. 128, no. 9, pp. 989-1000, 2002.
- [9] P. C. Hansen, "The use of the L-curve in the regularization of discrete ill-posed problems," *SIAM Journal on Scientific Computing*, vol. 14, no. 6, pp. 1457-1503, 1993.
- [10] S. S. Law and Y. L. Fang, "Moving force identification: Optimal state estimation approach," *Journal of Sound and Vibration*, vol. 239, no. 2, pp. 233-254, 2001.
- [11] S. S. Law, J. Q. Bu, X. Q. Zhu, and S. L. Chan, "Vehicle axle loads identification using finite element method," *Engineering Structures*, vol. 26, no. 8, pp. 1143-1153, 2004.
- [12] L. Yu and T. H. T. Chan, "Moving force identification from bending moment responses of bridge," *Structural Engineering and Mechanics*, vol. 14, no. 2, pp. 151-170, 2002.
- [13] T. Pinkaew, "Identification of vehicle axle loads from bridge responses using updated static component technique," *Engineering Structures*, vol. 28, no. 11, pp. 1599-1608, 2006.
- [14] P. Asnachinda and T. Pinkaew, "Experimental study on the identification of dynamic axle loads of moving vehicles from the bending moments of bridges," *Engineering Structures*, vol. 29, no. 9, pp. 2282-2293, 2007.
- [15] P. Asnachinda, T. Pinkaew, and J. A. Laman, "Multiple vehicle axle load identification from continuous bridge bending moment response," *Engineering Structures*, vol. 30, no. 10, pp. 2800-2817, 2008.
- [16] T. Deesomsuk and T. Pinkaew, "Effectiveness of vehicle weight estimation from bridge weigh-in-motion," *Advances in Civil Engineering*, vol. 2009, 2009, Art. no. 312034.
- [17] T. Deesomsuk and T. Pinkaew, "Evaluation of effectiveness of vehicle weight estimation using bridge weigh-in-motion," *The IES Journal Part A: Civil & Structural Engineering*, vol. 3, no. 2, pp. 96-110, 2010.
- [18] E. J. O'Brien, M. Quilligan, and R. Karoumi, "Calculating the influence line from direct measurement," *Proceedings of ICE – Bridge Engineering*, vol. 159, no. 1, pp. 31-34, 2006.
- [19] E. J. O'Brien, C. W. Rowley, A. Gonzalez, and M. F. Green, "A regularised solution to the bridge weigh-in-motion equations," *International Journal of Heavy Vehicle Systems*, vol. 16, no. 3, pp. 310-326, 2009.
- [20] H. Zhao, N. Uddin, and E. J. O'Brien, "Identification of vehicular axle weights with a bridge weigh-in-motion system considering transverse distribution of wheel loads," *Journal of Bridge Engineering ASCE*, vol. 19, no. 3, p. 04013008, 2014.
- [21] Z. Zhao, N. Uddin, and E. J. O'Brien, "Bridge weigh-in-motion algorithms based on the field calibrated simulation mode," *Journal of Infrastructure Systems ASCE*, vol. 23, no. 1, p. 04016021, 2017.
- [22] L. Deng and C. S. Cai, "Identification of dynamic vehicular axle loads: Theory and simulations," *Journal of Vibration Control*, vol. 16, no. 14, pp. 2167-2194, 2010.
- [23] L. Deng and C. S. Cai, "Identification of dynamic vehicular axle loads: Demonstration by a field study," *Journal of Vibration Control*, vol. 17, no. 2, pp. 183-195, 2010.
- [24] S. S. Leng, "Bridge influence line estimation for bridge weigh-in-motion system," *Journal of Computing in Civil Engineering*, vol. 29, no. 1, p. 06014006, 2015.
- [25] F. Carraro, M. S. Goncalves, R. H. Lopez, L. F. Miguel, and A. M. Valente, "Weight estimation on static B-WIM algorithms: A comparative study," *Engineering Structures*, vol. 198, p. 109463, 2019.
- [26] A. Znidaric and J. Kalin, "Using bridge weigh-in-motion systems to monitor single-span bridge influence lines," *Journal of Civil Structural Health Monitoring*, vol. 10, no. 5, pp. 743-756, 2020. [Online]. Available: <https://doi.org/10.1007/s13349-020-00407-2>
- [27] Z. Chen, T. H. T. Chan, and A. Nguyen, "Moving force identification based on modified preconditioned conjugated gradient method," *Journal of Sound and Vibration*, vol. 423, pp. 100-117, 2018.
- [28] C. D. Pan, L. Yu, H. L. Liu, Z. P. Chen, and W. F. Luo, "Moving force identification based on redundant concatenated dictionary and weighted l_1 -norm regularization," *Mechanical Systems and Signal Processing*, vol. 98, pp. 32-49, 2018.

- [29] Z. Chen, T. H. T. Chan, and L. Yu, "Comparison of regularization methods for moving force identification with ill-posed problems," *Journal of Sound and Vibration*, vol. 478, p. 115349, 2020.
- [30] R. J. Jiang, F. T. K. Au, and Y. K. Cheung, "Identification of masses moving on multi-span beams based on a genetic algorithm," *Computers and Structures*, vol. 81, pp. 2137-2148, 2003.
- [31] R. J. Jiang, F. T. K. Au, and Y. K. Cheung, "Identification of vehicles moving on continuous bridges with rough surface," *Journal of Sound and Vibration*, vol. 274, pp. 1045-1063, 2004.
- [32] S. Kim, J. Lee, M. S. Park, and B. W. Jo, "Vehicle signal analysis using artificial neural networks for a bridge weigh-in-motion system," *Sensors*, vol. 9, pp. 7943-7956, 2009.
- [33] Q. Zhang, L. Jankowski, and Z. Duan, "Simultaneous identification of moving vehicles and bridge damages considering road rough surface," *Mathematical Problems in Engineering*, vol. 2013, 2013, Art. no. 963424.
- [34] M. Lydon, S. Taylor, C. Doherty, D. Robinson, E. J. O'Brien, and A. Znidaric, "Bridge weigh-in-motion using fibre optic sensors," *Proceedings of ICE – Bridge Engineering*, vol. 170, no. 3, pp. 219-231, 2017.
- [35] E. A. Oskoui, T. Taylor, and F. Ansari, "Method and sensor for monitoring weight of trucks in motion based on bridge girder end rotations," *Structure and Infrastructure Engineering*, vol. 16, no. 3, pp. 481-494, 2020.
- [36] S. Z. Chen, G. Wu, and D. C. Feng, "Development of a bridge weigh-in-motion method considering the presence of multiple vehicles," *Engineering Structures*, vol. 191, pp. 724-739, 2019



Pattarapong Asnachinda received the B.Eng. in civil engineering from Chiang Mai University, Thailand in 2002, and M.Eng. and Ph.D. in civil engineering from Chulalongkorn University, Thailand, in 2004 and 2008, respectively.

From 2008, he was a lecturer in civil engineering, faculty of engineering, Burapha University, Thailand. Since 2019 he has been an assistant professor with the civil engineering department, faculty of engineering, Burapha University, Thailand. His research interests include structural dynamics and vibration, bridge weigh-in-motion, structural health monitoring, bridge structures, and structural engineering.



Tospol Pinkaew received the B.Eng. in civil engineering from Chulalongkorn University, Thailand in 1990, M.Eng. in structural engineering from Asian Institute of Technology, Thailand in 1992, and D.Eng. in civil engineering from University of Tokyo, Japan in 1995.

He is currently a professor with the civil engineering department, faculty of engineering, Chulalongkorn University, Thailand. His research interests include structural dynamics, vibration control of structures, wind and earthquake engineering, inelastic analysis of the reinforced concrete building, and infrastructure inspection and testing.